Markov Reliability Modeling for Induction Motor Drives under Field-Oriented Control

Ali M. Bazzi, *Member, IEEE*, Alejandro Dominguez-Garcia, *Member, IEEE*, and Philip T. Krein, *Fellow, IEEE*

***Abstract*— This paper presents a Markov reliability model of induction motor drives operating under field-oriented control. The model includes faults in the power electronics, machine, speed encoder, and current sensors. The procedure can be extended for more detail, to other machines, and to other drive topologies. To develop the model, faults are first identified, then a simulation model of the setup is developed and experimentally verified. Faults are injected into the model in sequential levels, and the system performance is assessed after each fault. Fault coverage—the probability that the system survives given a fault has occurred—is studied. A complete Markov reliability model is developed to assess the mean time to failure of the system and other reliability factors. This analysis is shown to be simple and useful for assessing the reliability of motor drives, and is expected to help in designing fault tolerance mechanisms for specific drives where reliability can be evaluated after every design.**

***Index Terms*— Markov reliability model, induction motor drive, fault impact assessment.**

I. Introduction

Reliability assessment of motor drives is essential, especially in electric transportation applications. Safety is a major concern in such applications, and it is tied directly to reliability. For example, a more reliable motor drive in an electric vehicle could enhance the vehicle's safety features. Industrial applications of motor drives require high reliability to maintain the functionality of manufacturing, pumping, cooling, and other processes. Since induction machines are the workhorses of industry and constitute at least 50% of global industrial load, and since they are being used in several transportation applications [1, 2], this paper proposes a method for reliability assessment of induction motor drives such as the one shown in Fig. 1. This method was introduced in [3] and can be extended to other machines, drives, and even other electrical systems.

Several reliability modeling techniques are available. These include reliability block diagrams (RBDs), fault trees, and Markov models. The reader is referred to [4] for a detailed discussion of each of these techniques. Among these techniques, Markov reliability modeling is the most powerful.

This is because it can capture many important features that RBDs and fault trees cannot. Examples are: sequences of faults in which the order matters, different repair strategies, fault coverage (the probability the system survives given that a fault has occurred), common mode failures, time-dependent failure rates, and state-dependent failure rates. Therefore, Markov reliability models are adopted in this paper.

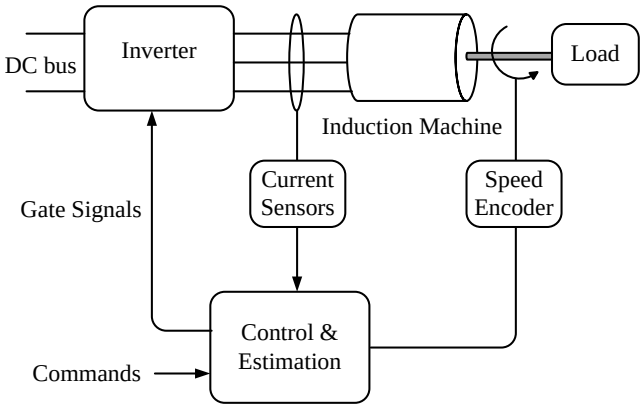

Fig. 1. Typical induction motor drive

Most reliability models can be extended to the component level or shrunk to high-level subsystems. For example, an encoder can be thought of as system on its own. It is possible to develop a model that explains specific sensor failure modes and traces them back to constituent components (resistors, capacitors, op-amps). If the encoder is part of a motor drive, and the interest is in understanding how the drive system behaves in the presence of faults, a sensor failure model that describes how the encoder output behaves for different internal faults without detailing the cause will suffice. The level of detail in any reliability analysis sets the complexity of the analysis, and more fault modes cause exponential growth of the system states.

In this paper, a complete framework for evaluating the reliability of an induction motor under indirect field-oriented control (IFOC) is presented. This framework is distinct from general reliability modeling procedures as those in [4] as it considers operational and reliability aspects of motor drives, including drive performance requirements fault modes in different drive components, while being easy to follow by designers and researchers in the power electronics and drives community. The proposed reliability model lays the

Authors are with the Grainger Center for Electric Machinery and Electromechanics, Department of Electrical and Computer Engineering, University of Illinois at Urbana-Champaign, Urbana, IL 61801 USA.

This work is supported by the Grainger Center for Electric Machinery and Electromechanics at the University of Illinois. This work is based on previous work entitled "A method for impact assessment of faults on the performance of field-oriented control drives: A first step to reliability modeling" presented at the IEEE Applied Power Electronics Conference, Palm Springs CA USA, Feb. 2010.

foundations of more sophisticated and advanced models that can be extended to different machines, drives, faults, and recovery or protection mechanisms. It combines several reliability concepts such Markov reliability modeling and fault coverage with a dynamic model of the overall system that enables coupling the impacts of component faults with the overall system dynamic performance. The faults studied here cover the power electronics, machine, and sensors, and the proposed framework gives the flexibility to go into a more detailed evaluation at the component level. This framework not only builds on available research in the field of reliability analysis of faults in higher-power components, e.g., broken rotor bars, but also includes faults in lower-power components such as those in sensors. The mathematical procedures for evaluating failure probabilities, survivor or reliability function, and mean time to failure (MTTF) are presented. It is well known that failure rates rely on published data that could be inaccurate due to different operating and testing conditions, component sizes, and conservative estimates, thus, failure rates used in this paper only imply an MTTF that is based on their values. MTTF results mentioned later in the paper do not necessarily reflect those of all drives, even of similar size, but rather reflect a case study. Therefore, failure rates of subsystems or components are left to final evaluation steps to provide more general results in which practitioners can plug in specific numbers; an example is presented here.

The paper proceeds as follows: Section II reviews available research on reliability of motor drives. Section III introduces relevant reliability modeling notions used throughout the paper. Fault modes of every subsystem in a motor drive are analyzed in Section IV. Section V portrays the proposed reliability modeling procedure. A simulation model is presented and validated with experiments in Section VI. All faults are then injected and system performance is evaluated in Section VII. The results from Section VII are used to build the Markov reliability model of a motor drive, and to calculate MTTF and $R(t)$ in Section VIII. Section IX concludes the paper.

II. Literature Review

While the literature contains significant work on important aspects of design for reliability and fault tolerance in induction motor drives, comprehensive tools to support systematic analysis and quantitative results have not been discussed. There are many excellent studies that define fault models. The objective of this paper is to create a framework for these models that will support systematic, quantitative analysis of fault impacts and design methods for fault mitigation. Faults include those in the inverter [5], control [6], power supply [7, 8], and motor [9]. Aspects of fault detection and isolation have been analyzed extensively as in [5, 10-17]. For example, pattern recognition is used in [13], while a short-time Fourier transform is used in [17] to identify faults. Redundancy has been investigated, with extensive work on multiphase motors [18] and split-wound motors [19]. At the control level, fault-tolerant control algorithms for permanent magnet synchronous machines (PMSMs) and induction machines have been presented in [5, 20-22]. Other strategies for improving the reliability of a system include reliable communication [23], preventive maintenance [24, 25], component de-rating, and component count reduction.

Extensive work has been conducted on fault-tolerant drives and motor control design, but literature on systematic methods for modeling and analysis of fault impacts on system operation and reliability is limited. It is essential to assess whether or not a design meets reliability and fault tolerance requirements for all possible operating conditions, and to compare different design choices. Reliability of the motor and supply is presented in [26], while component reliability analyses are presented in [27-29]. In [28], faults in control, power electronics, and the motor are addressed, while in [27] control faults are ignored and faults in the transformer and line filters are considered. The work presented in [29] also ignores control, but considers cooling faults.

Markov models are rarely applied in the context of motor drive reliability. In [30], only power electronics failures are considered, while in [31] the induction motor is considered as part of a larger power system. An excellent attempt to develop a Markov model of an induction motor drive is available in [32]. In this regard, even though sensors are subject to faults, these are ignored in the analysis presented there. Additionally, the criteria for declaring system failure, which are key for developing the reliability model, are not clearly defined. Sensor faults are studied in [33] for an automotive application where a multilayer control scheme is also addressed. Reference [34] proposes a method for reliability prediction for inverters in hybrid electric vehicles based on power loss estimation and standard failure rates. Even though basic reliability concepts are clearly defined, the proposed method only covers inverter reliability and is heavily model-dependent. The components of the inverter are assumed to have a series reliability structure, which is not clearly justified. Fault modes and effects analysis (FMEA) is used in [35], where fundamental reliability concepts are explained and applied to a redundant motor drive. Faults in power electronics, control signals, supply, and other components are all included in the analysis, but performance bounds are not clearly defined. The concept of fault coverage has not been thoroughly investigated in the available literature.

Therefore, most available literature is limited to physical faults, e.g., power electronics and machine faults, assumes certain system structures (from a reliability point of view), e.g., series components, and focuses on the development of fault tolerant control algorithms.

III. Preliminaries

A. Reliability Function, Mean Time to Failure, and the Exponential Distribution

Let T be a random variable describing the time to failure of a component. The component reliability at time t is defined as the probability that the component is still functional at time t [4], i.e., $R(t) = \Pr\{T > t\}$. The MTTF is then defined as

$$\text{MTTF} = \int_0^\infty R(\tau)d\tau \tag{1}$$

It is commonly assumed in reliability analysis that component failure is exponentially distributed. Thus, $R(t)$ is given by

$$R(t) = e^{-\lambda t}, \tag{2}$$

where λ is the so-called component failure rate. λ can be assumed to be constant even though it varies over time. The assumption of a constant λ comes from the "bath-tub" curve [4], where λ is constant for a period extending from the time after the initial commissioning of a component, to the time it significantly degrades and is more susceptible to failure. In the forthcoming analysis, the common assumption of constant λ assumes operating in the flat region of the bath-tub curve is used. The exponential distribution captures the expectation that as a component ages, its reliability decays to zero, and as $t \to \infty$, $R(t) \to 0$. For a single component, the MTTF is given by

$$\text{MTTF} = \frac{1}{\lambda}. \tag{3}$$

When series-parallel combinations of components exist, the combined reliability is not straightforward, and the exponential distribution simplifies the analysis. For example, for a series system with n components having failure rates $\lambda_1 \ldots \lambda_n$ and survivor functions $R_1(t) \ldots R_n(t)$, the overall reliability function and MTTF are given by

$$R(t) = \prod_{i=1}^{n} R_i(t) = e^{-\sum_{i=1}^{n} \lambda_i t}, \tag{4}$$

$$\text{MTTF} = \frac{1}{\sum_{i=1}^{n} \lambda_i}. \tag{5}$$

For n parallel connected components, the overall reliability function is given by

$$R(t) = 1 - \prod_{i=1}^{n} (1 - R_i(t)) = 1 - \prod_{i=1}^{n} (1 - e^{-\lambda_i t}), \tag{6}$$

and the MTTF can be calculated from (1).

B. Markov Processes

Loosely defined, a Markov process is a collection of random variables, indexed in time, taking values in some set called the state space, and satisfying the Markov property. This property requires that the future evolution of the process depends only on its current state. Let *X(t)* denote the collection of random variables defining the Markov process. Then, the probability P_{ij} of transitioning from state "*i*" at t = 0 to state "*j*" is defined as

$$P_{ij} = \Pr[X(t) = j \mid X(0) = i] \tag{7}$$

Given a set of possible states for *j*, the total probability of a transition to any *j* from *i*, plus the probability to stay at *i*, should add to 1. This is illustrated in Fig. 2, which also shows a third state "*k*" to which *X* can transition after *j*.

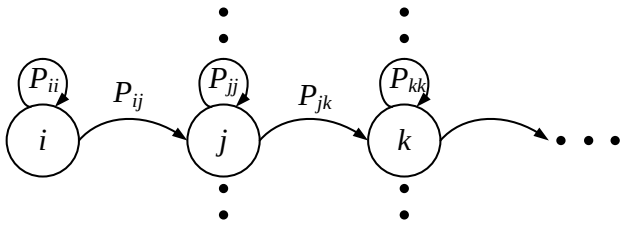

Fig. 2. Markov process

The possible transitions among different states of a Markov process can be described conveniently by a state-transition diagram as depicted in Fig. 2.

A probability matrix **P** can be built by setting its elements to the respective transition probabilities. For example, the probability of transitioning from *i* to *j* would be P_{ij} at the i^{th} row and j^{th} column of **P**. Given m+1 possible states of *X*, **P** can be constructed as

$$\mathbf{P}(t) = \begin{bmatrix} P_{00}(t) & P_{01}(t) & \cdot & \cdot & \cdot & P_{0m}(t) \\ P_{10}(t) & P_{11}(t) & \cdot & \cdot & \cdot & P_{1m}(t) \\ \cdot & \cdot & \cdot & & & \cdot \\ \cdot & \cdot & & \cdot & & \cdot \\ \cdot & \cdot & & & \cdot & \cdot \\ P_{m0}(t) & P_{m1}(t) & \cdot & \cdot & \cdot & P_{mm}(t) \end{bmatrix} \tag{8}$$

where the initial state is labeled *0* and the probabilities vary with time. The transition rates are given in a state transition matrix **Φ**, which is used to evaluate the probability dynamics. Relating this to a physical system, the initial state is always state 0, and **P** can be simplified to a row or column vector such as

$$\mathbf{P}(t) = \begin{bmatrix} P_0(t) & P_1(t) & \cdot & \cdot & \cdot & P_m(t) \end{bmatrix} \tag{9}$$

In the context of reliability modeling, the state-transition diagram associated with the Markov model describes the system status—failed or operational—for each system configuration reached after a unique sequence of component failures. The edges represent transitions between configurations triggered by component failures (or repair procedures). There are two types of nodes: *absorbing* nodes and *non-absorbing* nodes. The system will fulfill its function whenever it is in a non-absorbing node. The system will fail to deliver the functions for which it was designed whenever it transitions to an absorbing node. When a random fault occurs, the system transitions from one state to another. The transition rate is the failure rate of the component in which the fault occurred. A return to the previous state is referred to as *recovery*, and could have a *recovery rate* associated with it.

C. Chapman-Kolmogorov Equations

The probability of being in a given state at a given time is described by the Chapman-Kolmogorov equations

$$\dot{\mathbf{P}}^T(t) = \frac{d\mathbf{P}^T}{dt} = \mathbf{\Phi}^T \mathbf{P}^T(t) \tag{10}$$

The derivation of (10) is given in [4]. Solving this differential equation yields the probabilities of transitioning from every state to another as a function of time. The solution of (10) takes the form

$$\mathbf{P}^T(t) = e^{\Phi^T t}\mathbf{P}^T(0) \tag{11}$$

where $\mathbf{P}^T(0)$ is an $(m+1) \times 1$ vector, except for $P_0(0)=1$.

In a reliability analysis context, system reliability is quantified by calculating the probability that the system will be in any of the non-absorbing states at a given time. This can be accomplished easily by adding the entries of $\mathbf{P}^T(t)$ associated with non-absorbing states. In addition, the MTTF can be evaluated using (1).

D. Fault Coverage

The concept of fault coverage was introduced in response to the fact that it may not be possible to forecast with complete certainty whether a system will be able to deliver its function after a fault [36]. Fault coverage, denoted by c, can be interpreted as the conditional probability, given that a fault has occurred altering the system structure, that the system recovers and keeps delivering its intended function, i.e., c = Pr [system recovers | system fails].

For example, the response of a system to a component fault might differ depending on the operating conditions. In a dynamic system, operating conditions are governed by reference set points and external disturbances (a load in a motor drive is actually an external disturbance for the motor-drive dynamics). Thus, without loss of generality, assume that a system has an input u and a fault occurs at different values of u; assume that the system survives for 80% of the possible inputs, so the coverage for that fault is 80%. This is the probability that the system survives under that fault for different inputs.

Fault coverage can be included easily in a Markov reliability model, thus providing a link between the system dynamic behavior for different operating conditions and system reliability. In this regard, there are two possible outcomes after a component fault triggers a transition. In the Markov reliability model, this is reflected by transitions to two different states: one in which the system is still operational, and one in which it fails. The transition rate to the operational state is given by the product of the particular component failure rate and the fault coverage c. Similarly, the transition to a failed state is given by the product of the component failure rate and 1- c.

E. Example

Assume that when a fault occurs a system will survive and transition from state i to state j_1 with a probability of c where $0 \le c \le 1$ and represents the coverage. With probability (1-c), the system will fail and transition to j_2. Let the failure rate of this fault be λ_{ij}. Fig. 3 illustrates this part of the Markov model.

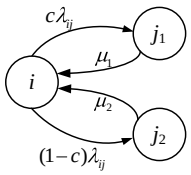

Fig. 3. Part of a Markov model showing fault coverage

The Markov model is a convenient way to find dynamic transition probabilities of the drive using (10), where $\mathbf{\Phi}$ is filled with the transition rates shown in Fig. 3. Calculation of the probabilities yields $R(t)$ and the MTTF. For the model shown in Fig. 3, repair rates μ_1 and μ_2 are shown as an example of how to build $\mathbf{\Phi}$. The resulting $\mathbf{\Phi}$ for the three states i, j_1, and j_2 is thus

$$\Phi = \begin{bmatrix} -c\lambda_{ij} - (1-c)\lambda_{ij} & c\lambda_{ij} & (1-c)\lambda_{ij} \\ \mu_1 & -\mu_1 & 0 \\ \mu_2 & 0 & -\mu_2 \end{bmatrix}.$$

IV. Motor Drive, Faults, and Performance

A. System Overview

An induction motor drive under IFOC requires measurements of the three-phase currents and speed, and has two control inputs for torque or speed and rotor flux. An induction machine under IFOC with hysteresis current control is shown in Fig. 4 [37]. In Fig. 4, ψ_{dr} is the direct-axis rotor flux linkage, and L_m and L_r are the magnetizing and rotor inductances, respectively. The rotor time constant is τ_r, n_p is the number of pole pairs, i_{ds} and i_{qs} are the d- and q-axis stator currents, respectively; i_{abc} are the three-phase stator currents, ρ is the electrical angle, ω_m is the mechanical speed, ω_r, ω_{sl}, and ω_s are the rotor, slip, and stator frequencies, respectively; and T_e is the electromechanical torque. The superscript * stands for a command value. Based on Fig. 4, faults can occur in six possible subsystems or components:

- Induction machine
- Inverter
- Current sensors
- Speed encoder
- Control and estimation platform
- Connectors and wires

The control and estimation platform, connectors, and wires are assumed to have very low failure rates compared to the rest of the system. This assumption is justified in part since the platform, which is usually a microcontroller, digital signal processor (DSP), or field programmable gate array (FPGA), is very reliable and does not involve high currents, high voltages, or mechanical movement. The wires and connectors are static and should have low failure rates, except in high-vibration or corrosive environments, if selected and installed correctly. The procedure proposed later can augment these subsystems into the reliability model, but this is not included here for the sake of simplicity.

The motor drive under study includes a 400 V / 100 A inverter connected to a 230 V, four-pole, 1.5 hp induction machine with rated speed of 1750 rpm at 60 Hz. Motor

parameters are shown in Table A-I in the appendix. The ratings of the machine help develop the allowable currents, voltages, speed, torque, and flux in the machine. All control and estimation is done on a DSP. Details regarding simulation and experimental setups are presented in Section VI.

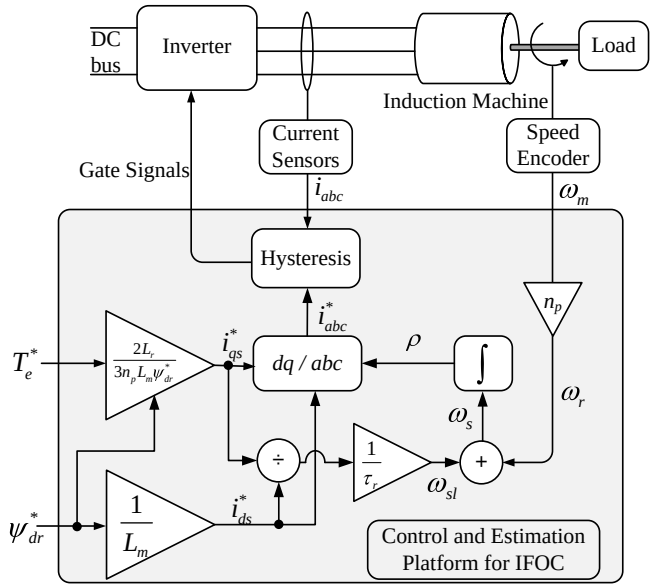

Fig. 4. Induction motor drive under IFOC

B. Fault Modes

Machine, inverter, current sensor, and speed encoder faults are considered. Even though literature is rich with analysis and diagnostics of machine and power electronics faults, sensor faults are rarely addressed in drive applications. Current sensor and encoder faults include omission (loss of signal), incorrect gain, and constant value (unresponsive signal), in addition to bias in current sensors. More discussion of faults and models is presented in Section VI.

Inverter faults addressed here are at the IGBT-diode module level, and include short circuits (SC) to ground, SC to the dc voltage bus, and open circuits (OC) [5, 18, 30]. Lower level circuitry such as gate drivers, and passive components such as inductors and link capacitors, are assumed to have low failure rates that have little impact on the system. Electrolytic capacitors are an exception, since they have relatively rapid degradation with time.

Since the motor under study is a squirrel-cage induction motor, broken rotor bars or rings need to be considered [38]. Motor faults studied here include phase-to-phase faults and broken rotor bars, which are the most common faults in induction machines. Motor OC and SC faults are considered in the inverter. The faults are summarized in Table I.

TABLE I
MAJOR FAULTS IN MAIN SUBSYSTEMS

	Speed Encoder	Current Sensor	Phase Leg	Motor
Fault Types	• Omission (SEO) • Gain (SEG) • Constant (SEC)	• Omission (CSO) • Gain (CSG) • Bias (CSB) • Constant (CSC)	• OC • SC to ground (SCG) • SC to dc bus (SCDC)	• Phase to phase fault (PP) • Broken rotor bar (BR)

Component redundancy is not considered in this study since it is rare in off-the-shelf motor drives. When analyzing the faults, only phase *a* power electronics and current sensor faults are considered owing to symmetry among the three phases. This inherent symmetry can help with fault detection and isolation, in addition to predicting the shapes and values of healthy signals.

C. Performance Evaluation

System performance criteria are essential in determining whether performance is acceptable. After every fault, system performance is evaluated based on performance measures. These metrics can be functional, such as state overshoot or settling time, or non-functional, such as total energy consumption or cost. In a motor drive, these measures should consider the safety of the operator, e.g. passengers in an electric vehicle, and safety of the motor drive itself. Examples of performance measures and associated requirements for driving conveyors are presented in [38].

A general depiction of two performance measures, pm_1 and pm_2, is shown in Fig. 5. The shaded rectangle labeled *A* shows the actual performance of the system while the rectangle labeled *B* shows the acceptable bounds on each performance measures. If *A* is enclosed by *B* then the system performance is acceptable, otherwise, the system has failed.

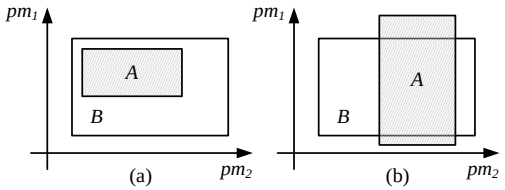

Fig. 5. (a) System survival within performance bounds, (b) system failure outside performance bounds

For each system configuration arising from different faults, performance measures are analyzed. Even though these measures are useful in determining whether each possible system configuration has failed or not, it is necessary to define an aggregated reliability measure using a Markov model. In an IFOC motor drive, performance measures include the machine speed and torque, stator current peak, and settling time of all of these. Bounds are set based on desired operational limits.

V. METHODOLOGY

The reliability modeling methodology for a motor drive proceeds in simple steps. The first step is to define the essential system components or subsystems. These are elements that can fail frequently, and can affect system operation. Whether the whole system would later fail or not is part of the observations. After these components are determined, possible fault modes are analyzed, e.g. OC or SC faults in an IGBT-diode module. The fault modes can be expanded into a long list, but basic or common faults should be considered. The motor drive will be operating under certain conditions with desired performance characteristics. These conditions and operational characteristics are used to set performance bounds. For example, the torque on the motor

shaft set by the pedal in an electric vehicle should be bounded within certain limits, and once it exceeds these limits, over-speeding or sudden braking could occur.

Once performance bounds are set, a test platform can be used to study the effect of faults on the drive. Faults are injected into the system one by one, and critical variables are monitored and recorded. A fault could be followed by another, thus "fault cascading" would result in multiple fault levels. Given N vulnerable components in a system, each with K faults, the result is K^N fault combinations. Therefore, fault combinations grow exponentially as component counts increase. Authors in [34] state that "adding components reduces reliability," but this is not always true. When components are added for redundancy, reliability can increase, but the reliability analysis and modeling becomes more complex. The analysis is simplified when only a few fault levels are considered, as most systems would not survive multiple sequential faults.

After the first level of faults is injected and critical variables are recorded, these variables are compared to the performance bounds. If any variable exceeds its allowed bounds, the system is considered in a "failure" state, otherwise it has survived. If the system survives, another level of faults is injected after the first fault, and the analysis repeats. In the study presented later here, two fault levels are considered and the rest are truncated into a failure state. The error between this truncation and the actual levels can be estimated. Varying one or more inputs and repeating the fault injection and evaluation analysis provides the fault coverage of the drive. Once all fault combinations are analyzed and fault coverage is found, a Markov model or a state transition diagram can be built.

VI. Simulation and Experiments

The implementation of the proposed methodology in both simulation and experiments is essential to find the MTTF of a motor drive. Even though applying this methodology in experiments could be enough to find the complete reliability model, some of the faults could damage the experimental setup and cannot be tested directly. Also, many commercial motor drives have built-in protection circuitry and algorithms that take action after a fault by shutting down or otherwise altering operation. It is not easy (or advisable) to override protection, but fault modes used here can also integrate protection in several aspects. For example, an OC fault can be the result of a protection circuit tripping one phase due to over-current in that phase. The ability of a protection and fault detection circuit to protect and recover the system can also be integrated to the Markov model through recovery action with recovery rates. This is not considered here due to the unavailability of published recovery rates which is not the case for failure rates, and because the main focus of this paper is to develop a systematic procedure to develop a reliability model of induction motor drives. Numerical simulations can tolerate severe faults and extreme operating conditions, avoid protection algorithms except as a design evaluation, and provide a suitable environment for fault injection and performance evaluation. An important step before starting the reliability modeling methodology is to validate the simulation model against experiments. Even though the simulations here do not model or cover all physical dynamics, noise, vibration, power loss, and nonlinearities of material, they provide a useful tool that can save the cost of rebuilding a motor drive, or most other systems, after severe failures.

A. Simulations

Simulations of the IFOC induction motor drive shown in Fig. 4 were done in MATLAB/Simulink® for a 1.5 hp induction machine. The inverter involved IGBT-diode pairs from the SimPowerSystems Toolbox in Simulink, and the load torque was modeled as quadratic in speed. Quadratic loads include fans, aerodynamic drag, and propulsion based on the propeller law. Alternative load models are possible. Two major fault types are simulated: faults on the power side in the inverter and machine, and faults on the sensor side.

SC faults are modeled by shorting lines with an ideal switch. A challenge with ideal switches in simulations is the abrupt change of state. This can be resolved by adding a snubber resistor across the switch whose value is close to an open circuit. Fig. 6 shows the simulated model with switches that emulate the SC to dc bus, SC to ground, and phase-to-phase faults. The OC fault is injected inside the inverter model. The broken rotor bar fault requires more detail where rotor currents, resistances, and inductances are modified when the fault happens. A simple version increases the rotor resistance because rotor bars are modeled as parallel resistors joined at the ends. To simplify the analysis, inductances are ignored [39]. Even though the machine under study is a squirrel-cage machine, a shorted-wound-rotor model is used to access the rotor resistances and modify them under a broken rotor bar fault. The block in Fig. 6 labeled "Step3" models a broken rotor bar fault by increasing the rotor resistance.

The second set of faults, sensor faults, includes the current sensors and speed encoder. Only one current sensor is considered in this analysis since the other two yield similar results. As mentioned in Section IV, current sensor faults include omission, gain, bias, and constant, while speed encoder faults include these except for bias. Omission is modeled by setting the sensor output to zero. Gain is modeled by applying a numerical gain to the sensor signal, where the sensor output is amplified or attenuated due to an internal fault or due to a fault in its interface circuitry. A sensor could also get stuck at a constant value if the interface circuit fails or saturates, e.g. saturation of a magnetic core or a ground wire break. Bias of the sensor could occur and can be solved by calibration. It can also be inherent in current sensors as shown in Fig. 7 where the actual sensor output has an offset and ranges from $V_{sense,min}$ to $V_{sense,max}$. The interface circuit would adjust for this offset but the adjustment is not perfect. Values for the gain, constant, and bias faults are shown in Table II. The sensor fault model used is similar to the model proposed in [40], and is shown in Fig. 8.

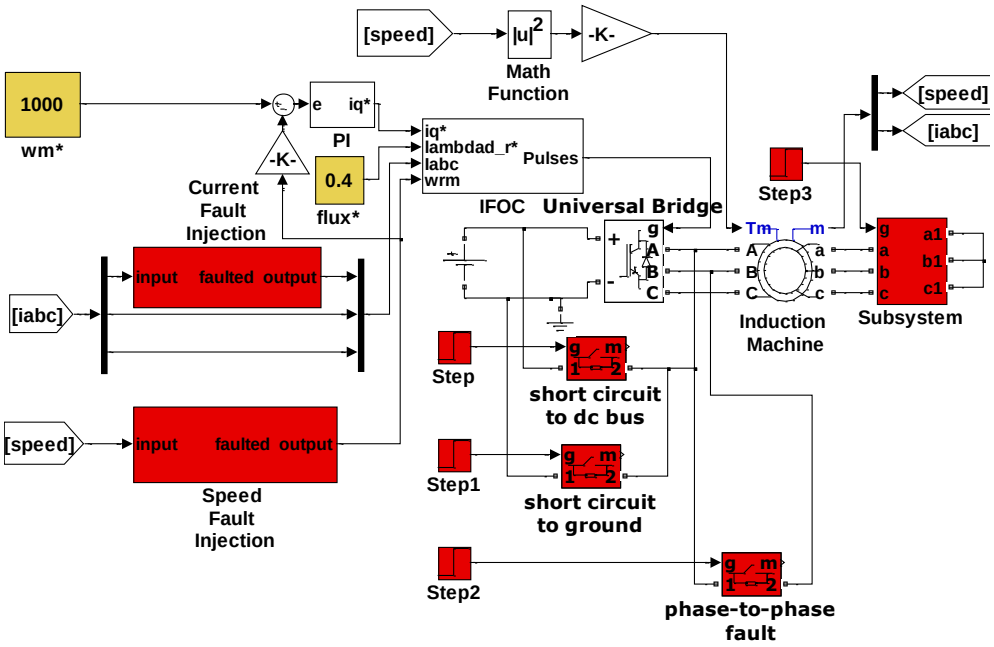

Fig. 6. Simulink model of the IFOC induction motor drive with faults

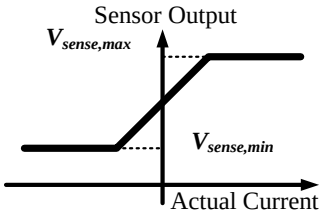

Fig. 7. Typical current sensor output voltage versus actual current

The model in Fig. 8 provides the flexibility of changing the gain, bias, and constant values. It also includes a time setting for the "Switch" at which the fault is injected.

TABLE II
VALUES USED WITH FAULTS IN SENSORS

Fault Type	Speed Encoder	Current Sensor
Gain	1.5	1.5
Constant	900 rpm	3 A
Bias		+1 A

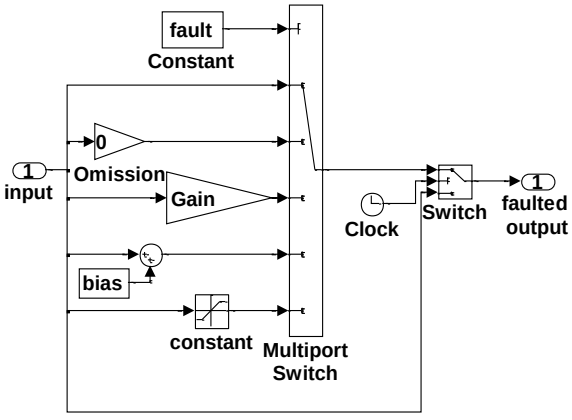

Fig. 8. Current sensor and encoder fault model

B. Experiments and Model Validation

A squirrel cage induction machine, inverter, and control were implemented experimentally to validate the model. IFOC with real-time control and monitoring is built on an eZdspF2812™ platform [41] which includes a Texas Instruments TMS320F2812 DSP. This control platform is integrated in the inverter [42]. The experimental setup is shown in Fig. 9. The dynamometer shown in Fig. 9 sets the load torque.

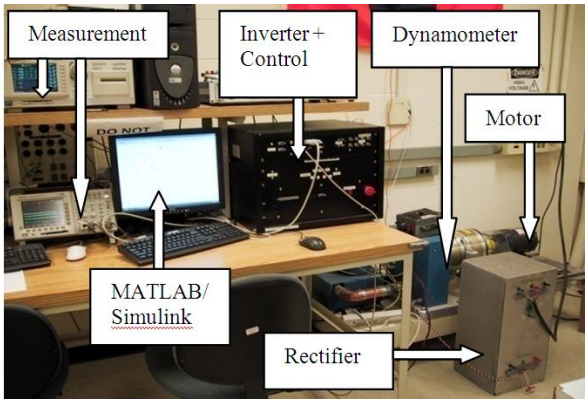

Fig. 9. Experimental setup for model validation

Simulations and experiments of the motor drive at 1000 rpm with a 2 N·m load were used to validate the model. Different faults were injected at t = 2 s. To protect the experimental setup without significantly affecting the model, two factors were considered. The first factor is to avoid injecting faults that could cause severe failures or trigger the protection circuitry as predicted from simulations. The second factor is to use a tight external closed-loop torque control in experiments to avoid sudden overload conditions on the dynamometer and

the motor shaft. This loop is not needed in simulations. Figures 10–13 show the simulation and experimental results for two faults among several that were tested. The faults shown are speed encoder omission, current sensor constant, and an OC fault.

Results show that the model is valid and generally behaves as expected from experiments. In the result of the OC fault, the current in the simulations is not zero because of the added snubber resistance. Experimental results show that the current before any fault has a peak of 9 A on average, but simulation results show a peak of 5 A. This discrepancy is due to the small hysteresis band in simulations that cannot be set in experiments. Note that the model is almost perfect under faults, which is the main goal of the modeling process.

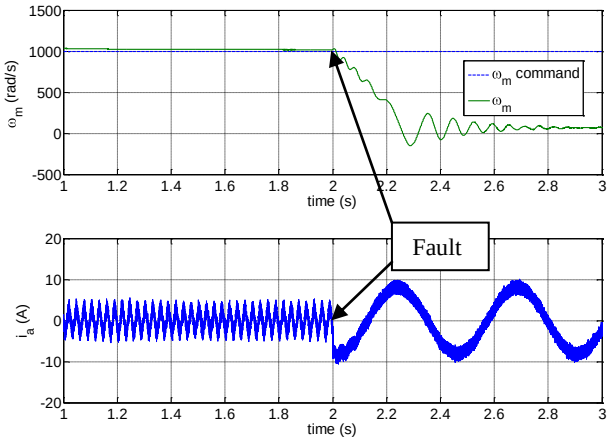

Fig. 10. Simulation results for speed encoder omission: Actual and command speed (500 rpm/div, top), current in phase *a* (10A/div, bottom).

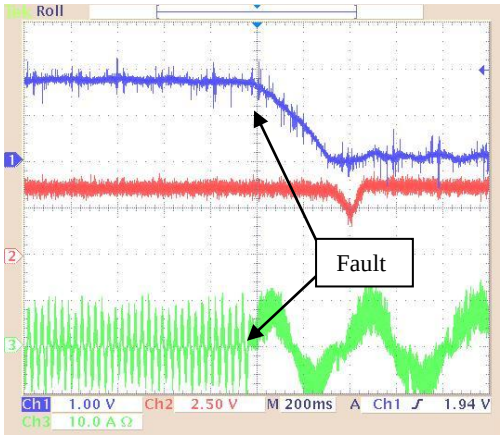

Fig. 11. Experimental results for speed encoder omission: Speed (500 rpm/div, top), torque (2 N·m/div, middle) current in phase *a* (10A/div, bottom).

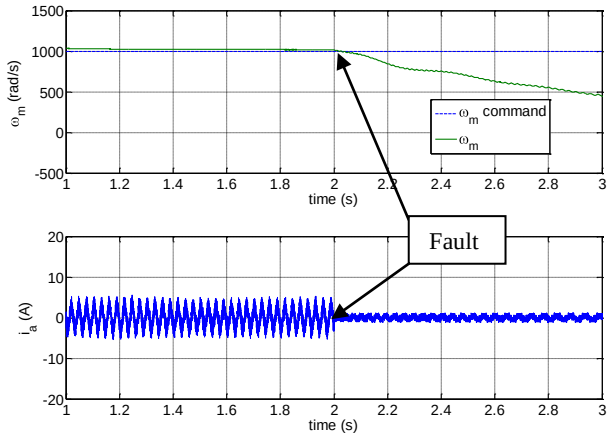

Fig. 12. Simulation results for OC in phase *a*: Waveforms and scales as Fig. 10.

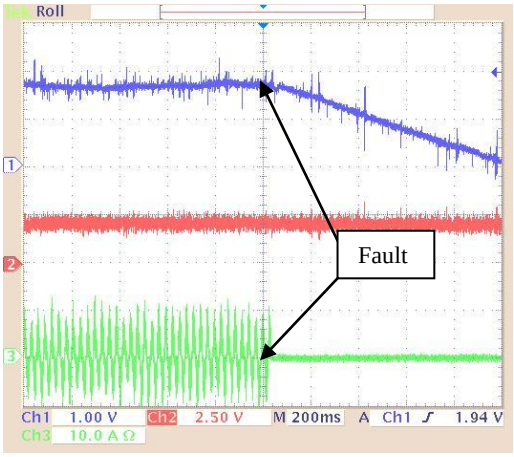

Fig. 13. Experimental results for OC in phase *a*: Waveforms and scales as Fig. 11.

VII. Multiple Fault Injection and Performance Evaluation

Since the simulation model was validated under faults, all faults were injected into the model and the system response was monitored. After a fault occurs, if the system survives and reaches steady-state, another fault is injected as a "second fault level." Performance measures are set for speed, peak current, and settling time. Torque, voltage, and other performance measures can be included if desired. The bounds used are shown in Table III.

TABLE III
Performance Bounds

Speed	Command speed ± 50 rpm
Current	-10 A ≤ Peak ≤ 10 A
Settling time	≤ 250 ms

Table IV shows the system status after the first fault level. The system survived for seven faults, including one with 80% coverage, and failed for five. For the seven faults that were survived, a second fault is injected in another component. Results for the second fault level are shown in Table V. Since

only one fault is assumed to occur in any single component in a fault sequence, second faults in that component are not applicable (NA). Also, IFOC accepts two inputs and fault coverage must be tested for an allowed range of input values. The torque or speed input of IFOC sets the operating point; the flux linkage input is varied to model both over-rated flux operation and flux weakening. Here the rated flux linkage is 0.5 V·s. Flux linkage values from 0.2 V·s to 0.6 V·s were tested for fault coverage. The speed or torque input is held constant but fault coverage over a speed range can be studied in a similar manner. The fractions shown in some of the cells in Tables IV and V reflect the coverage — the probability of survival after a fault. When an omitted current sensor (CSO) was the first fault, it caused the system to fail for a flux input of 0.6 V·s, but the system survived for the four other inputs; therefore, it has a coverage of 4/5 at the first fault level. If a component fails at the first level, then by definition, the system cannot survive any second-level faults. In Tables IV and V, *F* indicates failure, *S* indicates survival, and the fault acronyms are from Table I.

TABLE IV
SYSTEM STATUS AFTER THE FIRST FAULT LEVEL

Fault 1	Status
SEO	*F*
SEG	*F*
SEC	*F*
CSO	*S*, c_1=4/5
CSG	*S*
CSB	*S*
CSC	*F*
SCDC	*S*
SCG	*S*
OC	*F*
PP	*S*
BR	*S*

TABLE V
SYSTEM STATUS AFTER THE SECOND FAULT LEVEL

	Fault 1						
Fault 2	CSO	CSG	CSB	SCDC	SCG	PP	BR
SEO	*F*	*F*	*F*	*F*	*F*	*F*	*F*
SEG	*F*	*F*	*F*	*F*	*F*	*F*	*F*
SEC	*F*	*S*	*F*	*F*	*F*	*F*	*F*
CSO	NA	NA	NA	*S*, c_5=4/5	*S*, c_7=4/5	*S*	*S*, c_9=2/5
CSG	NA	NA	NA	*S*	*S*	*S*	*S*
CSB	NA	NA	NA	*S*	*S*	*S*	*S*
CSC	NA	NA	NA	*S*	*F*	*S*, c_8=3/5	*F*
SCDC	*S*, c_3=1/2	*S*	*S*	NA	NA	*S*	*S*
SCG	*S*, c_2=3/4	*S*	*S*	NA	NA	*S*	*S*
OC	*F*	*F*	*F*	NA	NA	*F*	*F*
PP	*S*, c_3=1/2	*S*	*S*	*S*, c_4=2/5	*S*, c_6=2/5	NA	NA
BR	*S*, c_3=1/2	*S*	*S*	*S*	*S*	NA	NA

Results show that the system fails under several faults even at the first level, so fault tolerant control algorithms, sensor redundancy, sensorless control, and other reliability enhancement methods should be considered. Some of the results are near the performance bounds, which means that allowing modest performance degradation will increase survival under some faults.

Information about the drive status after every fault is extracted from Tables IV and V to build the Markov model. For example, there are eight states after a fault occurs in the initial state: seven states in which the drive survives (shown in Table IV as survived), while the eighth is a failure state that lumps all failed states in Table IV. Fault coverage and failure rates are used to build the complete Markov model as in the example shown in Fig. 3.

VIII. RELIABILITY MODEL

A. Nominal Condition and Dominant Faults

Based on fault injection results and performance analysis, a system either survives or fails under the first fault or second fault. To limit complexity of the analysis, the system is assumed to be in a failure state following a third fault. In a procedure similar to that followed for Fig. 3, the Markov model of the system is built but without considering recovery. The model includes 52 states: one initial state, seven survival states after "Fault 1", one failed state after "Fault 1" that lumps five failures, 35 states that survived after "Fault 2" including states that survived only for certain inputs, seven failed states that occur after each survival under "Fault 1," and one failed state at the third fault level. To solve for the probabilities, the rows and columns of the absorbing states, nine failure states in this case (one + seven + one, as mentioned above), are eliminated from **Φ**, which becomes 43 x 43 matrix. **Φ** is a sparse matrix since not all states in the state-transition diagram are connected. The diagram is not shown here due to space limitations, but the non-zero elements of **Φ** are listed in Table A-II in the appendix. Failure rates are labeled as λ with the fault names as subscripts. Once **Φ** is known, the probabilities can be found using (11), and their sum would be the reliability or survivor function $R(t)$. The failure rates given in Table VI were extracted from [32, 43-46], and can be used to find $R(t)$. Notice that the failure rates used here are collected from the literature, and more accurate failure rates can be used without affecting the methodology.

TABLE VI
ILLUSTRATIVE FAILURE RATES

Failure Rate	failures/hour	Failure Rate	failures/hour
λ_{SEO}	7.4×10^{-7}	λ_{CSC}	1×10^{-7}
λ_{SEG}	1.9×10^{-7}	λ_{OC}	5×10^{-7}
λ_{SEC}	1.9×10^{-7}	λ_{SCG}	5×10^{-7}
λ_{CSO}	1×10^{-7}	λ_{SCDC}	5×10^{-7}
λ_{CSG}	1×10^{-7}	λ_{PP}	3.2×10^{-6}
λ_{CSB}	1×10^{-7}	λ_{BR}	3.2×10^{-6}

Solving for **P** for the values in Table VI using Mathematica® gives $R(t)$,

$$\begin{aligned} R(t) = {} & 2.585e^{-9.65\times10^{-6}t} - 1.052e^{-9.25\times10^{-6}t} - 1.0167e^{-8.15\times10^{-6}t} \\ & + 0.008042e^{-7.9\times10^{-6}t} + 0.522e^{-7.75\times10^{-6}t} - 1.4167e^{-3.25\times10^{-6}t} \\ & + 0.742e^{-2.85\times10^{-6}t} + 0.629e^{-1.75\times10^{-6}t} + 0.7(-e^{-9.65\times10^{-6}t} + e^{-9.25\times10^{-6}t}) \\ & + \frac{2}{3}(-e^{-9.65\times10^{-6}t} + e^{-8.15\times10^{-6}t}) - e^{-9.65\times10^{-6}t} + e^{-3.25\times10^{-6}t} \end{aligned} \quad (12)$$

Using (1) and the values in Table VI, the MTTF is found to be 501×10^3 hours or 57.2 years. $R(t)$ is expected to be

monotonically decreasing over time. This is illustrated in Fig. 14. This MTTF seems to suggest that electric drives can be sufficiently reliable in vehicle and other transportation applications.

In many practical systems, a few faults tend to dominate the MTTF. Dominant faults can be found analytically by solving for the eigenvalues of $\mathbf{\Phi}$ or by setting the failure rates of different faults to a very small number one at a time, and noting which faults cause drastic changes in $R(t)$. The dominant faults in the motor drive were found to be those associated with the speed encoder. An $R_{se}(t)$ function that only includes encoder failures is found and overlaid along with $R(t)$ in Fig. 14. The MTTF in this case is 742 × 10^3 hours. Based on areas in Fig. 14, encoder faults represent about 68% of the overall reliability impact. This motivates work on speed-sensorless control, although other faults have substantial impact and need to be addressed.

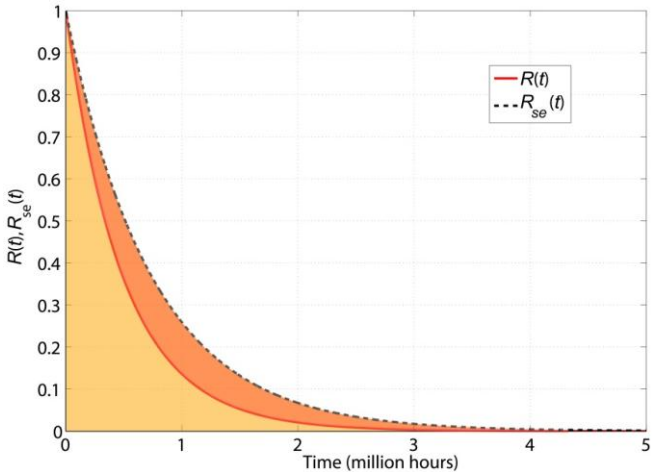

Fig. 14. $R(t)$ and $R_{se}(t)$ over time

Another way to simplify the analysis is to separate effects into high and low failure rates, λ_{high} and λ_{low}, where λ_{high} is on the order of 10^{-6} failures/hour and λ_{low} is on the order of 10^{-7} failures/hour. For $\lambda_{low}=3\times10^{-7}$ failures/hour (found from averaging all failure rates on the order of 10^{-7}) and $\lambda_{high}=3.2\times10^{-6}$ failures/hour, the resulting MTTF is 581 x 10^3 hours. The resulting error is less than 16%. The resulting reliability function, $R_s(t)$, is

$$\begin{aligned} R_s(t) = {} & 0.277e^{(-9.4\times10^{-6}t)} - 0.35e^{(-8.5\times10^{-6}t)} - 0.4e^{(-8.2\times10^{-6}t)} \\ & + 0.521e^{(-7.3\times10^{-6}t)} - 0.417e^{(-3\times10^{-6}t)} \\ & + 0.642e^{(-2.1\times10^{-6}t)} + 0.726^{(-1.8\times10^{-6}t)} \end{aligned} \quad , \quad (13)$$

but not plotted as it almost overlaps $R(t)$.

B. Effect of Sensor Fault Levels

Table II shows nominal values for different sensor faults, but the choice of these values can affect the MTTF resulting from the reliability model. In order to address this issue, different constant, bias, and gain values were considered, and the drive MTTF was found. Ideally the no-fault conditions for sensor faults are SEG=1, CSG=1, and CSB=0 while SEC and CSC should not exist as the sensor can never be stuck at a constant due to sinusoidal currents and speed ripple. Values of SEG, SEC, CSG, CSC, and CSB are swept over a range. When one value sis being swept, other values are left as shown in Table II. The nominal fault conditions in Table II are highlighted in Table VII, and different MTTFs resulting from several sensor fault values are tabulated in Table VII except for the SEG which had no significant change on the MTTF. It is clear from Table VII that SEC causes lower MTTFs as cause farther from the actual speed of 1000RPM. Also, as the CSG moves away from the no-fault condition CSG=1, the MTTF decreases. Table VII also shows that as the CSC moves away from a median value of 3 A, and as the bias reduces the actual current measurement, the MTTF decreases. While the MTTF change reported in Table VII is not very significant, it shows that the choice of sensor fault values can affect the final reliability model and MTTF result.

TABLE VIII
EFFECT OF SENSOR FAULT VALUES

SEC	MTTF (hours × 10^3)	CSG	MTTF (hours × 10^3)	CSC	MTTF (hours × 10^3)	CSB	MTTF (hours × 10^3)
700	497	0.5	497	1	500	-2	497
800	499	1.5	501	2	500	-1	497
900	501	2	496	3	501	1	501
1100	501	2.5	495	4	500	2	501
				5	500		

Another aspect of sensor faults was studied: In smaller drives, two current sensors are usually used to reduce the drive cost and size. The assumption in all previous analyses is that three current sensors exist, which is very reasonable for larger drives. In order to study the effect of having two sensors rather than three, the simulation model was modified such that readings from current sensors on phases a and b were used to infer the current in phase c for a balanced machine such that $i_c=-i_a-i_b$. The reliability modeling procedure considering all faults in Table I with nominal faults from Table II with two current sensors rather than three resulted in an MTTF that is higher by around 1%. The higher MTTF might not be intuitive given that there is one less sensor in the system, but the fact that i_c now compensates for any deficiencies in i_a due to the loss of the phase-a current sensor means that the current required to maintain the machine at its desire speed is forced to be drawn from phase c. Therefore, there is no clear conclusion on whether using three sensors is necessarily advantageous when compared to two sensors assuming a balanced machine.

In general, the proposed methodology for modeling the motor drive reliability results in conventional reliability measures: **P**, $R(t)$, and MTTF. Since the solutions are found analytically, failure probabilities and the reliability function can be predicted for any time t. Also, the script written in Mathematica and used to solve (10) is flexible where the structure of $\mathbf{\Phi}$ and the failure rates can be modified easily.

IX. CONCLUSION

The proposed methodology for reliability modeling covers essential faults in a drive system, including the machine,

power electronics, and sensors. The methodology leads to a Markov reliability model of an induction motor drive under IFOC, and can be extended to other drives or to more faults in other components. A model was validated in experiments and used for the complete procedure. The survivor function of the complete system was found analytically including fault coverage. Simplifications were proposed based on dominant fault modes, which were found to be faults in the speed encoder, and on a high-low failure rate approach. Failure rates from the literature suggest MTTF values on the order of 500,000 hrs for complete drives. The development of speed-sensorless control can be linked to the dominance of speed encoder failure rates.

Further research could apply this methodology to other drive topologies, more components in any topology (e.g. link capacitors, gate drives, etc.), design of fault tolerance, and actual field failure rates. Even though Markov models use a fixed failure rate, which might not be accurate since failure rates generally vary with time, the proposed methodology serves the purpose of a comprehensive, straightforward, and versatile reliability modeling procedure.

APPENDIX

TABLE A-I
MOTOR PARAMETERS

Motor Parameter	Value
Rated power	1.5 hp
Rated speed	1750 rpm
Number of poles (P)	4
Referred rotor resistance (R_r)	0.7309 Ω
Stator resistance (R_s)	1.5293 Ω
Referred rotor leakage inductance (L_{lr})	0.005343 H
Stator leakage inductance (L_{ls})	0.00356 H
Magnetizing inductance (L_m)	0.19778 H
Core Loss (R_c)	505 Ω
Inertia (J)	0.01 kg.m^2

TABLE A-II
NON-ZERO ELEMENTS OF THE STATE TRANSITION MATRIX

Element	Value
$\mathbf{\Phi}[1,1]$	$-(c_1\lambda_{CSO} + \lambda_{CSG} + \lambda_{CSB} + \lambda_{SCDC} + \lambda_{SCG} + \lambda_{PP} + \lambda_{BR} + \lambda_{F1})$
$\mathbf{\Phi}[1,2]$	$c_1\lambda_{CSO}$
$\mathbf{\Phi}[2,2]$	$-(c_3\lambda_{SCDC} + c_2\lambda_{SCG} + c_3\lambda_{PP} + c_3\lambda_{BR} + \lambda_{F2})$
$\mathbf{\Phi}[2,9]$	$c_3\lambda_{SCDC}$
$\mathbf{\Phi}[2,10]$	$c_2\lambda_{SCG}$
$\mathbf{\Phi}[2,11]$	$c_3\lambda_{PP}$
$\mathbf{\Phi}[2,12]$	$c_3\lambda_{BR}$
$\mathbf{\Phi}[3,3]$	$-(\lambda_{SEC} + \lambda_{SCDC} + \lambda_{SCG} + \lambda_{PP} + \lambda_{BR} + \lambda_{F3})$
$\mathbf{\Phi}[3,13]$	λ_{SEC}
$\mathbf{\Phi}[4,4]$	$-(\lambda_{SCDC} + \lambda_{SCG} + \lambda_{PP} + \lambda_{BR} + \lambda_{F4})$
$\mathbf{\Phi}[5,5]$	$-(\lambda_{CSC} + \lambda_{CSG} + \lambda_{CSB} + c_5\lambda_{CSO} + c_4\lambda_{PP} + \lambda_{BR} + \lambda_{F5})$
$\mathbf{\Phi}[5,23]$	$c_4\lambda_{PP}$
$\mathbf{\Phi}[5,24]$	λ_{CSC}
$\mathbf{\Phi}[5,26]$	$c_5\lambda_{CSO}$
$\mathbf{\Phi}[6,6]$	$-(c_7\lambda_{CSO} + \lambda_{CSG} + \lambda_{CSB} + c_6\lambda_{PP} + \lambda_{BR} + \lambda_{F6})$
$\mathbf{\Phi}[6,28]$	$c_7\lambda_{CSO}$
$\mathbf{\Phi}[6,31]$	$c_6\lambda_{PP}$
$\mathbf{\Phi}[7,7]$	$-(\lambda_{CSO} + \lambda_{CSG} + \lambda_{CSB} + c_8\lambda_{CSC} + \lambda_{SCDC} + \lambda_{SCG} + \lambda_{F7})$
$\mathbf{\Phi}[7,33]$	λ_{CSO}
$\mathbf{\Phi}[7,36]$	$c_8\lambda_{CSC}$
$\mathbf{\Phi}[8,8]$	$-(c_9\lambda_{CSO} + \lambda_{CSG} + \lambda_{CSB} + \lambda_{SCDC} + \lambda_{SCG} + \lambda_{F8})$
$\mathbf{\Phi}[8,39]$	$c_9\lambda_{CSO}$
$\mathbf{\Phi}[1,3]$, $\mathbf{\Phi}[5,25]$, $\mathbf{\Phi}[6,29]$, $\mathbf{\Phi}[7,34]$, $\mathbf{\Phi}[8,40]$	λ_{CSG}
$\mathbf{\Phi}[1,4]$, $\mathbf{\Phi}[5,27]$, $\mathbf{\Phi}[6,30]$, $\mathbf{\Phi}[7,35]$, $\mathbf{\Phi}[8,41]$	λ_{CSB}
$\mathbf{\Phi}[1,5]$, $\mathbf{\Phi}[3,14]$, $\mathbf{\Phi}[4,21]$, $\mathbf{\Phi}[7,37]$, $\mathbf{\Phi}[8,42]$	λ_{SCDC}
$\mathbf{\Phi}[1,6]$, $\mathbf{\Phi}[3,15]$, $\mathbf{\Phi}[4,20]$, $\mathbf{\Phi}[7,38]$, $\mathbf{\Phi}[8,43]$	λ_{SCG}
$\mathbf{\Phi}[1,7]$, $\mathbf{\Phi}[3,16]$, $\mathbf{\Phi}[4,19]$	λ_{PP}
$\mathbf{\Phi}[1,8]$, $\mathbf{\Phi}[3,17]$, $\mathbf{\Phi}[4,18]$, $\mathbf{\Phi}[5,22]$, $\mathbf{\Phi}[6,32]$	λ_{BR}
Diagonal elements $\mathbf{\Phi}[i,i]$, i=9, 10, 14, 15, 20, 21, 24– 30.	$\lambda_{SEC} + \lambda_{SEO} + \lambda_{SEG} + \lambda_{PP} + \lambda_{BR}$
Diagonal elements $\mathbf{\Phi}[i,i]$, i=11, 12, 16–19, 33–36, 39–41.	$\lambda_{SEC} + \lambda_{SEO} + \lambda_{SEG} + \lambda_{SCDC} + \lambda_{SCG} + \lambda_{OC}$
$\mathbf{\Phi}[13,13]$	$\lambda_{SCDC} + \lambda_{SCG} + \lambda_{OC} + \lambda_{PP} + \lambda_{BR}$
Diagonal elements $\mathbf{\Phi}[i,i]$, i=22, 23, 31, 32, 37, 38, 42, 43.	$\lambda_{SEC} + \lambda_{SEO} + \lambda_{SEG} + \lambda_{OC} + \lambda_{CSG} + \lambda_{CSB} + \lambda_{CSC}$

REFERENCES

[1] Available: "http://www.greencar.com/articles/20-truths-gm-ev1-electric-car.php".

[2] Available: "http://www.teslamotors.com/performance/perf_specs.php."

[3] A.M. Bazzi, A.D. Dominguez-Garcia, and P.T. Krein, "A method for impact assessment of faults on the performance of field-oriented control drives: A first step to reliability modeling", in *Proc. IEEE Applied Power Electron. Conf. Expo.*, 2010, pp. 256-263.

[4] M. Rausand and A. Høyland, System Reliability Theory: Models, Statistical Methods, and Applications, 2nd ed. Hoboken, NJ: Wiley, 2005.

[5] D. Kastha and B. K. Bose, "Investigation of fault modes of voltage-fed inverter system for induction motor drive," *IEEE Trans. Ind. Appl.*, vol. 30, pp. 1028-1038, July/Aug. 1994.

[6] J. Pontt, J. Rodriguez, J. Rebolledo, L. S. Martin, E. Cid, and G. Figueroa, "High-power LCI grinding mill drive under faulty conditions," in *Proc. Ind. Applicat. Conf.*, 2005, pp. 670-673.

[7] R. M. Tallam, D. W. Schlegel, and F. L. Hoadley, "Failure mode for AC drives on high resistance grounded systems," in *IEEE Appl. Power Electron. Conf. Expo.*, 2006, pp. 1587-1591.

[8] Y. Yuexin and A. Y. Wu, "Transient response of electric drives under utility upset conditions," in *Proc. Pulp and Paper Ind. Tech. Conf.*, 1996, pp. 77-85.

[9] V. P. Shevchuk, "Investigations of the operation reliability increase of the alternating current electric machines in diamond extractive industries," in *Proc. Int. Scientific and Practical Conf. of Students, Post-graduates and Young Scientists: Modern Technique and Technologies*, 2002, pp. 103-104.

[10] A. Fekih and F. N. Chowdhury, "A Fault Tolerant Control Design for Induction Motors," in *Proc. IEEE Int. Conf. on Syst., Man and Cybern.*, 2005, pp. 1320-1325.

[11] S. Green, D. J. Atkinson, A. G. Jack, B. C. Mecrow, and A. King, "Sensorless operation of a fault tolerant PM drive," *IEE Proc. on Elect. Power Applicat.*, vol. 150, pp. 117-125, 2003.

[12] O. Jasim, C. Gerada, M. Sumner, and J. Arellano-Padilla, "Investigation of induction machine phase open circuit faults using a simplified

equivalent circuit model," in Proc. Int. Conf. on Elect. Mach., 2008, pp. 1-6.

[13] K. S. Lee and J. S. Ryu, "Instrument fault detection and compensation scheme for direct torque controlled induction motor drives," *IEE Proc. Control Theory and Applicat.*, vol. 150, pp. 376-382, 2003.

[14] O. Ondel, G. Clerc, E. Boutleux, and E. Blanco, "Fault Detection and Diagnosis in a Set "Inverter-Induction Machine" Through Multidimensional Membership Function and Pattern Recognition," *IEEE Trans. Energy Convers.*, vol. 24, pp. 431-441, June 2009.

[15] R. L. A. Ribeiro, C. B. Jacobina, E. R. C. Da Silva, and A. M. N. Lima, "Compensation strategies in the PWM-VSI topology for a fault tolerant induction motor drive system," in *Proc. IEEE Int. Symp. on Diagnostics for Elect. Mach., Power Electron. and Drives*, 2003, pp. 211-216.

[16] R. B. Sepe, Jr., B. Fahimi, C. Morrison, and J. M. Miller, "Fault tolerant operation of induction motor drives with automatic controller reconfiguration," in *Proc. IEEE Int. Elect. Mach. and Drives Conf.*, 2001, pp. 156-162.

[17] W. G. Zanardelli, E. G. Strangas, and S. Aviyente, "Identification of Intermittent Electrical and Mechanical Faults in Permanent-Magnet AC Drives Based on Time-Frequency Analysis," *IEEE Trans. Ind. Appl.*, vol. 43, pp. 971-980, July/Aug. 2007.

[18] M. T. Abolhassani and H. A. Toliyat, "Fault tolerant permanent magnet motor drives for electric vehicles," in *Proc. IEEE Int. Elect. Mach. and Drives Conf.*, 2009, pp. 1146-1152.

[19] J. C. Salmon and B. W. Williams, "A split-wound induction motor design to improve the reliability of PWM inverter drives," *IEEE Trans. Ind. Appl.*, vol. 26, pp. 143-150, Jan./Feb. 1990.

[20] J. W. Bennett, A. G. Jack, B. C. Mecrow, D. J. Atkinson, C. Sewell, and G. Mason, "Fault-tolerant control architecture for an electrical actuator," in *Proc. IEEE Power Electron. Specialists Conf.*, 2004, pp. 4371-4377.

[21] O. Wallmark, L. Harnefors, and O. Carlson, "Control Algorithms for a Fault-Tolerant PMSM Drive," *IEEE Trans. Ind. Electron*., vol. 54, pp. 1973-1980, Aug. 2007.

[22] A.W. Williams, "High reliability 3-phase variable-frequency inverter," *IEE Proc. on Electric Power Applicat*., vol. 129, pp. 353-354, 1982.

[23] S. Bolognani, L. Peretti, L. Ssgarbossa, and M. Zigliotto, "Improvements in Power Line Communication Reliability for Electric Drives by Random PWM Techniques," in *Proc. IEEE Ind. Electron. Conf.*, 2006, pp. 2307-2312.

[24] G. F. D'Addio, S. Savio, and P. Firpo, "Optimized reliability centered maintenance of vehicles electrical drives for high speed railway applications," in Proc. *IEEE Int. Symp. on Ind. Electron*., 1997, pp. 555-560 vol.2.

[25] F. A. DeWinter, R. Paes, R. Vermaas, and C. Gilks. (2002, Jul./Aug.). Maximizing large drive availability. *IEEE Ind. Appl. Mag. pp*. 66-75.

[26] J. A. Oliver and D. Poteet, "High-speed, high-horsepower electric motors for pipeline compressors: available ASD technology, reliability, harmonic control," *IEEE Trans. Energy Convers.*, vol. 10, pp. 470-476, Sep. 1995.

[27] R. Bozzo, V. Fazio, and S. Savio, "Power electronics reliability and stochastic performances of innovative ac traction drives: a comparative analysis," in *Proc. IEEE Power Tech. Conf.*, 2003, p. 7.

[28] R. D. Klug and M. Griggs, "Reliability and availability of megawatt drive concepts," in *Proc. Int. Conf. on Power Syst. Tech*., 2004, pp. 665-671.

[29] P. Wikstrom, L. A. Terens, and H. Kobi, "Reliability, availability, and maintainability of high-power variable-speed drive systems," *IEEE Trans. Ind. Appl*., vol. 36, pp. 231-241, Jan./Feb. 2000.

[30] R. Letchmanan, J. T. Economou, A. Tsourdos, I. A. Ashokaraj, and B. A. White, "Fault Evaluation of Relative-Coupled BLDC Drives for Multi-Facet Mobile Robot with Distributed Speed Factors," in *Proc. IEEE Veh. Power and Propulsion Conf.*, 2006, pp. 1-6.

[31] M. H. J. Bollen and P. M. E. Dirix, "Simple model for post-fault motor behaviour for reliability/power quality assessment of industrial power systems," *IEE Proc. Generation, Transmission and Distribution*, vol. 143, pp. 56-60, 1996.

[32] M. Molaei, H. Oraee, and M. Fotuhi-Firuzabad, "Markov Model of Drive-Motor Systems for Reliability Calculation," in *Proc. IEEE Int. Symp. on Ind. Electron.*, 2006, pp. 2286-2291.

[33] W. Hainan, S. Pekarek, and B. Fahimi, "Multilayer control of an induction motor drive:A strategic step for automotive applications," *IEEE Trans. Power Electron*., vol. 21, pp. 676-686, May 2006.

[34] A. Hirschmann, D. Tissen, S. Schroder, and R. W. De Doncker, "Reliability Prediction for Inverters in Hybrid Electrical Vehicles," *IEEE Trans Power Electron.*, vol. 22, pp. 2511-2517, Nov. 2007.

[35] K. J. P. Macken, I. T. Wallace, and M. H. J. Bollen, "Reliability Assessment of Motor Drives," in *Proc. IEEE Power Electron. Specialists Conf.*, 2006, pp. 1-7.

[36] W. G. Bouricius, W. C. Carter, and P. R. Schneider, "Reliability modeling techniques for self-repairing computer systems," in *Proc. ACM Annu. Conf./ Annu. Meeting*, 1969, pp. 295-309.

[37] P. C. Krause, O. Wasynczuk, and S. D. Sudhoff, Analysis of Electric Machinery and Drive Systems, 2nd ed. New York: Wiley - IEEE Press, 2002.

[38] K. D. Jackson, M. D. McCulloch, and C. F. Landy, "A study of the suitability of electric drives to the task of driving conveyors," in *Proc. IEEE Ind. Applicat. Soc. Annu. Meeting*, 1993, pp. 488-495.

[39] A.F. Alshandoli, "Model-Predicted Induction Motor Behaviour under Different Operating Conditions," in *Proc. Int. Conf. on Elect. Eng*., 2007, pp. 1-7.

[40] A.D. Domínguez-García, J. G. Kassakian, J. E. Schindall, and J. J. Zinchuk, "An Integrated Methodology for the Dynamic Performance and Reliability Evaluation of Fault-Tolerant Systems," *J. Reliab. Eng. and Syst. Safety*, vol. 93, pp. 1628-1649, Nov. 2008.

[41] eZdspF2812TM Technical Reference. 506265-0001 Rev. F. Spectrum Digital. Stafford, TX. 2003.

[42] J. Kimball, M. Amerhein, A. Kwasinski, J. Mossoba, B. Nee, Z. Sorchini, W. Weaver, J. Weels, and G. Zhang, "Modular Inverter for Advanced Control Applications," Univ. of Illinois, IL, Rep. CEME-TR-200-01, 2006, .

[43] IEEE Standard Reliability Data for Pumps and Drivers, Valve Actuators, and Valves, ANSI/IEEE Standard 500, 1984.

[44] Military Handbook Reliability Prediction of Electronics Equipment, MIL-HDBK-217F, 1995.

[45] R. Bozzo, V. Fazio, and S. Savio, "Power electronics reliability and stochastic performances of innovative ac traction drives: a comparative analysis," in *Proc. IEEE Bologna Power Tech. Conf.*, 2003, p. 7.

[46] A. Ristow, M. Begovic, A. Pregelj, and A. Rohatgi, "Development of a Methodology for Improving Photovoltaic Inverter Reliability," *IEEE Trans. Ind. Electron.*, vol. 55, pp. 2581-2592, July 2008.